

Employing synthesized Zn-based photocatalysts for degradation of Rhodamine B in an aqueous environment

Mojdeh Zargaran^a, Majid Abdouss^{b,*}, Hamidreza Abdouss^c, Aref Shokri^{d,e,*}

^aRoad, Housing and Urban Development Research Center, Tehran, Iran, email: m.zargaran@bhrc.ac.ir

^bChemical Group, Amirkabir University of Technology, Tehran, Iran, email: phdabdouss44@aut.ac.ir

^cDepartment of Polymer Engineering and Color Technology, Amirkabir University of Technology, Tehran, Iran, email: hamidrezaabdouss@gmail.com

^dDepartment of Chemistry, Payame Noor University (PNU), Tehran, Iran, email: aref.shokri3@gmail.com

^eJundi-Shapur Research Institute, Dezfoul, Iran

Received 30 November 2020; Accepted 26 June 2021

ABSTRACT

In this study, three different types of Zn-based catalysts, including ZnAl₂O₄, ZnAl₂O₄/SiO₂ and ZnAl₂O₄/CNT (CNT – carbon nanotube) photocatalysts, were synthesized by the hydrothermal method. The successful synthesis and properties of the photocatalysts were investigated by infrared spectroscopy, X-ray diffraction, field-emission scanning electron microscopy (FESEM), X-ray scattering energy, energy-dispersive X-ray analysis, nitrogen adsorption–desorption and photoluminescence (PL) spectroscopy. Then their efficiencies on the degradation of Rhodamine B dye were studied. The characterization tests have shown that the samples are correctly synthesized. Through FESEM, it was clear that the size of ZnAl₂O₄/CNT nanoparticles was smaller than that of ZnAl₂O₄/SiO₂ and consequently its surface area was greater. Nitrogen adsorption–desorption analysis showed that the ZnAl₂O₄/CNT sample has a higher surface area compared to ZnAl₂O₄/SiO₂, which provides more improvement in photocatalytic activity. The PL test showed that in ZnAl₂O₄/CNT sample, the electron–hole pair recombination rate was lower and the separation efficiency was many times higher, which increased the photocatalytic activity of ZnAl₂O₄/CNT. Finally, it was shown that the dye was completely removed by ZnAl₂O₄/CNT along with UV-light compared to other photocatalysts after 15 min of exposure.

Keywords: Zn nanocomposite; Photocatalytic degradation; Rhodamine B; Hydrothermal method; Carbon nanotube

1. Introduction

Through the quick advance in leather, textile, paper and food industries, dye pollutants of different water resources have increased extreme distresses due to their carcinogenicity and toxicity [1]. Thus, it is essential that dye pollutants must be eliminated from aqueous media before releasing them into the environment [2]. The photocatalysts are an effective method to degrade the dye pollutant molecule [3,4]. The textile industries consume

large amounts of water and are one of the largest water-consuming industries. The amount of water consumed in these industries varies between 1 to 3 cubic meters per ton of product depending on the type of production process. Dyes are a group of complex organic materials that enter the environment at various stages in the textile industry. Therefore, color pollutants are one of the primary sources of organic contaminants in the textile industry and their conversion to harmless materials is essential. Inhalation of these compounds often causes respiratory disorders

* Corresponding author.

and direct contact with them can cause local burns, eye injuries, increased sweating and mental illnesses [5,6].

Rhodamine B is a cationic dye, highly water-soluble and acidic property due to the presence of the carboxylic acid group. Due to its intense color and durability, it is widely used in the textile industry and is discharged into sewage streams. In the absence of oxygen, these dyes form toxic substances that threaten human health and the water ecosystem, thus removing these hazardous dyes to create a clean and healthy environment is important [7].

An ideal treatment method for water and wastewater involves the decomposition of available toxins which should also be cost-effective and efficient. The advanced oxidation processes (AOPs) are referred to as oxidative processes, which are mainly based on the interference of hydroxyl radicals in the reaction of pollutant decomposition. The photocatalytic process is a branch of AOPs that produces hydroxyl radicals to react with resistant pollutants [8–11].

In recent years, metal oxides such as WO_3 , CdS , Fe_2O_3 , SnO_2 , ZnS , ZnO , and TiO_2 have received the most studies in the field of photocatalytic reactions. This can be attributed to the low cost of these oxides, the appropriate optical and electrical properties, non-toxicity and the chemical stability of these compounds [12,13]. Titanium dioxide-based heterogeneous photocatalysts have received the most attention, but it has some disadvantages. The TiO_2 bandgap is approximately 3.2 eV, thus a large bandgap prevents the absorption of visible light in photocatalytic reactions. Since only about three to five percent of sunlight forms the UV portion, inactivation by esophageal radiation is one of the significant limitations of this photocatalyst. On the other hand, electron–hole coupling recombination is performed very fast in titanium dioxide. These disadvantages limit the use of TiO_2 in photocatalytic reactions and clarify the need for alternative compounds [14–16].

Carbon nanotubes have been an essential part of nanotechnology in recent years. These nanomaterials have unique physical and chemical properties that will make them increasingly applicable. High absorption power is one of the factors for their application in environmental activities. Carbon nanotubes have a higher adsorption capacity than other compounds, such as porous graphite carbon. Another prominent feature of these materials is the high surface-to-volume ratio of these adsorbents, which has a significant impact on their use as adsorbents [17]. Multi-walled carbon nanotubes have a fullerene (ball-like) structure with large layers of carbon atoms. The surface of these nanotubes has a high tendency to react with other molecules and atoms, so these adsorbents can absorb pollutants several times as active carbon [18].

Carbon nanotubes had a high adsorption capacity to remove methyl orange and methyl blue dyes of 1 and 2 mg g^{-1} , respectively. Many studies have been done on the removal of dyes by carbon nanotubes [19].

In this study, three different types of zinc-based catalysts, including ZnAl_2O_4 , $\text{ZnAl}_2\text{O}_4/\text{SiO}_2$ and $\text{ZnAl}_2\text{O}_4/\text{CNT}$ (CNT – carbon nanotube) photocatalysts, were synthesized by hydrothermal method. Then their properties were investigated by infrared (IR) spectroscopy, X-ray diffraction (XRD), energy-dispersive X-ray analysis (EDX), field-emission scanning electron microscopy (FESEM),

nitrogen adsorption–desorption and photoluminescence (PL) spectroscopy. Finally, the efficiencies of these photocatalysts on the degradation of Rhodamine B dye in the aqueous environment were investigated.

2. Materials and methods

2.1. Materials and equipment

Nine-hydrated aluminum nitrate, six-hydrated zinc-nitrate, sodium hydroxide, carbon nanotube, and silicon oxide were purchased from Aldrich Company in America and used to synthesize photocatalysts. The Rhodamine B dye was purchased from Merck Company in Germany. All chemicals employed were of analytical grade and used without further purification as received. The X-ray diffraction investigations were executed on a Bruker D8 ADVANCE X-ray diffractometer. Infrared spectra were logged on a Shimadzu System FTIR-8400 spectrophotometer applying the KBr pellet manner. The UV-Visible spectrophotometry is a Lambda 25 model from PerkinElmer (USA), which records the spectrum in 200–800 nm. The used FESEM device was the German ZEISS SIGMA VP model. The 2001 D8 ADVANCE model of the XRD device was used to determine the properties of precursors and the synthesized catalysts in the laboratory.

The specific surface area was considered through the Brunauer–Emmett–Teller (BET) technique by N_2 adsorption–desorption tests performed at -196°C on a Micromeritics ASAP 2010. The sample was outgassed at 200°C for 3 h, before each measurement. EDX, EDX-7000/8000, prepared by the Shimadzu Company in Japanese, was employed to recognize the elemental composition of synthesized catalysts.

2.2. Synthesis of ZnAl_2O_4 by hydrothermal method

A wet chemical solution method is the hydrothermal technique using low temperatures to create nanometric catalysts directly with narrow size distribution and high surface areas without the need for later thermal treatments [20]. About 10 mL of an aqueous solution containing six-hydrated Zn-nitrate (10 mmol, 2.975 g) was added to a 10 mL aqueous solution of nine-hydrated aluminum nitrate (20 mmol, 7.503 g). Then, 0.1 M sodium hydroxide solution was added to the solution containing salts. Hydroxide sodium solution was added to adjust the pH range of 9–10. The resulting mixture was stirred at 50°C for an hour and then transferred to a 100 mL hydrothermal autoclave container and incubated at 180°C for 18 h. After the hydrothermal process, the autoclave cooled to ambient temperature. The sample was then filtered and washed twice with distilled water. The resulting precipitate was dried at 100°C for 2 h.

2.3. Synthesis of $\text{ZnAl}_2\text{O}_4/\text{CNT}$ and $\text{ZnAl}_2\text{O}_4/\text{SiO}_2$ composite by hydrothermal method

ZnAl_2O_4 based catalysts can be prepared by sol–gel [21], co-precipitation [22] and hydrothermal methods. First, 5 mL of nanotube carbon suspension with an initial concentration of 25 mg mL^{-1} was subjected to ultrasonic waves for 1 h. 10 mL of aqueous solution on six-hydrated

zinc nitrate (10 mmol, 2.975 g) was added to 10 mL aqueous solution of nine-hydrated aluminum nitrate (20 mmol, 7.503 g). The dispersed nanotube carbon mixture was added to humans containing soluble salts and then 0.1 M hydroxide sodium solution drop was added. Hydroxide sodium solution was added to adjust the pH range from 9.5 to 10.0. The resulting mixture was stirred at 50°C for 1 h and then transferred to a 100 mL hydrothermal autoclave container and incubated at 180°C for 18 h. After the hydrothermal process, the autoclave cooled to ambient temperature. The sample was then filtered and washed twice with distilled water and ethanol. The resulting precipitate was dried at 100°C for 2 h.

The synthesis method of $\text{ZnAl}_2\text{O}_4/\text{SiO}_2$ composite is similar to that of the previous one, using 5 mL of silicon oxide suspension containing 25 mg mL^{-1} of silicon oxide in catalyst synthesis.

3. Results and discussion

3.1. Identification of synthesized catalysts

Different identification methods were used to identify the synthesized photocatalysts. Understanding the characteristics of the built-in catalysts is important for investigating their work. To study the structure and morphology of catalysts, identification techniques including IR spectroscopy, XRD, scanning electron microscopy (SEM), X-ray scattering energy and nitrogen adsorption–desorption were used.

3.2. Infrared spectroscopy of the samples

A series of absorption peaks in the range of 400–4,000 cm^{-1} were showed by Fourier-transform infrared spectroscopy (FTIR) spectra. The functional groups present in the catalysts can be realized due to the specific frequencies of the absorption peaks. The molecular structure characteristics

of the samples were identified by FTIR spectra. The infrared spectrum of functionalized carbon nanotubes is illustrated in Fig. 1a. The peak at 3,434 cm^{-1} corresponds to the tensile vibration of the hydroxyl group. The 2,924 and 2,857 cm^{-1} peaks are related to the tensile vibration of the $-\text{CH}_2$ group and the 1,390 and 1,457 cm^{-1} peaks are related to the flexural vibration of the $-\text{CH}_2$ group. The peaks of 1,630 and 1,113 cm^{-1} are related to the tensile vibrations of C=C and C–O carboxylic acid groups, respectively [23].

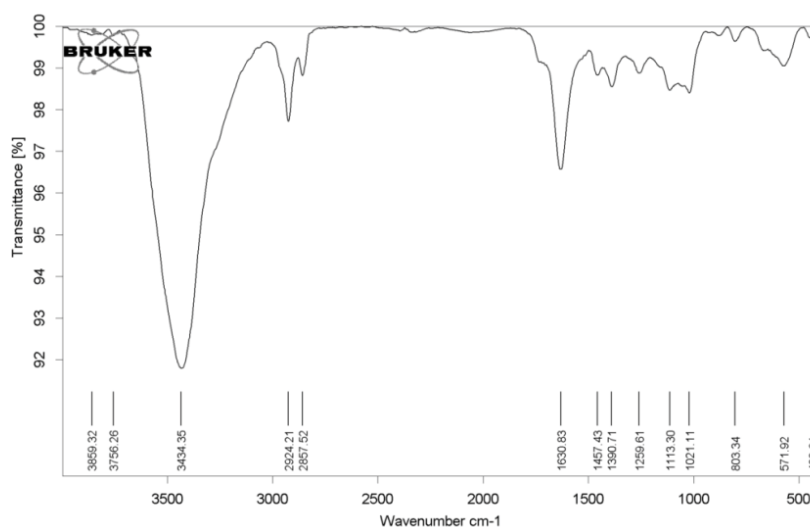
According to the FTIR spectrum of the ZnAl_2O_4 sample, the peak around 1,630 cm^{-1} and three peaks in the 1,670–470 cm^{-1} area are related to the HOH bending vibration of the absorbed water, the symmetric tensile Al–O vibration, the symmetric tensile Al–O vibration, and the asymmetric Al–O tensile vibration (Fig. 1b). These peaks are triple peaks of the regular spinel structure and the aluminum centers with octahedral coordinates which present in all synthesized photocatalyst samples [24,25].

The spectrum of $\text{ZnAl}_2\text{O}_4/\text{CNT}$ is shown in Fig. 1c which is a combination of the infrared spectra of ZnAl_2O_4 and CNT. As it can be seen from Fig. 1d, the FTIR spectrum of the $\text{ZnAl}_2\text{O}_4/\text{SiO}_2$ sample showed the peak in the 1,670–470 cm^{-1} area that is related to Al–O symmetric tensile vibration, and Al–O symmetric flexural vibration. The peak at 440 to 450 is associated with the bending vibrations of the O–Si–O bond and at 790 to 800 is to the symmetric tensile vibrations of the O–Si–O bond [26].

3.3. X-ray diffraction study of synthesized photocatalysts

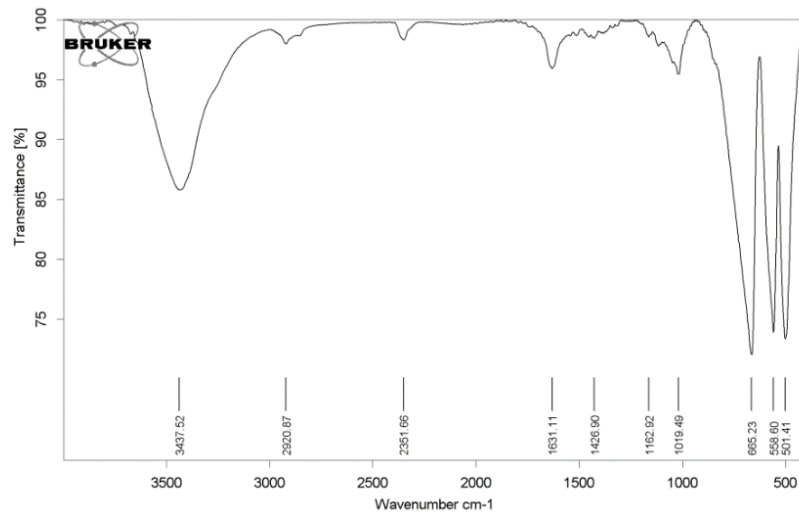
The crystal structure of the samples was investigated by X-ray diffraction via Cu $K\alpha$ radiation ($\lambda = 0.15418 \text{ nm}$). The specimens were examined in angular range ($2\theta = 10^\circ\text{--}90^\circ$). All patterns matched the standard templates.

The X-ray diffraction pattern of ZnAl_2O_4 showed a good agreement with the X-ray diffraction pattern of card

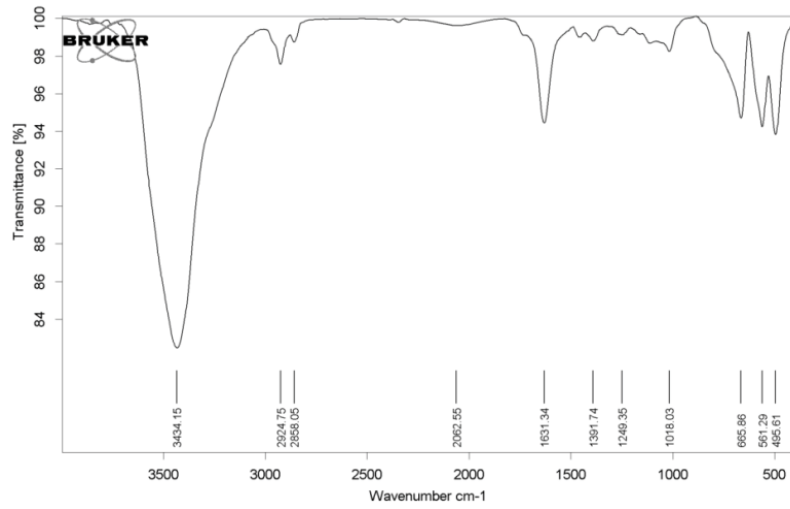


(a)

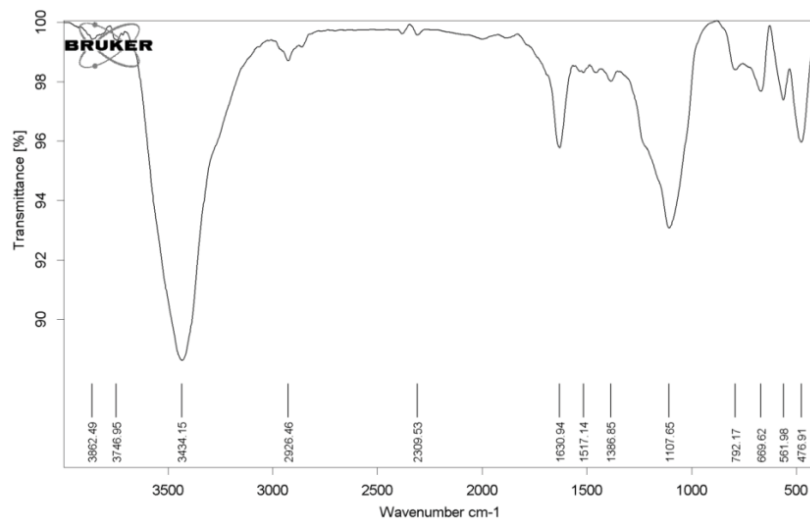
Fig. 1. (a) IR spectrum of carbon nanotube.



(b)



(c)



(d)

Fig. 1. (b) IR spectrum of ZnAl_2O_4 , (c) IR spectrum of $\text{ZnAl}_2\text{O}_4/\text{CNT}$, and (d) IR spectrum of $\text{ZnAl}_2\text{O}_4/\text{SiO}_2$.

number [1961-073-01] on aluminum oxide. The X-ray diffraction pattern of $\text{ZnAl}_2\text{O}_4/\text{CNT}$ showed a good match with the X-ray diffraction pattern of card number [0669-005-00]. Also, the X-ray diffraction pattern of $\text{ZnAl}_2\text{O}_4/\text{SiO}_2$ showed a good agreement with the X-ray diffraction pattern of card number [1036-082-01]. As presented by other researchers, the ordered preparation and crystallinity of the synthesized sample can be explored over XRD results [27].

3.4. Using SEM test for the synthesized catalysts

In SEM analysis, a sample was scanned with an electron beam to create a magnified image for analysis. The morphology of the synthesized photocatalysts is shown as carbon nanotubes as rods on the substrate in Fig. 2.

The photocatalyst was prepared through the hydrothermal method with a small particles size. The micrographs of ZnAl_2O_4 and $\text{ZnAl}_2\text{O}_4/\text{CNT}$ attained by SEM are presented in Fig. 3a–d, respectively. The micrograph of ZnAl_2O_4 (Fig. 3a and b) exposed agglomerated particles with the morphology of shaped plate type and minor aggregates on the surface of larger clusters [28]. The SEM images of $\text{ZnAl}_2\text{O}_4/\text{CNT}$ and $\text{ZnAl}_2\text{O}_4/\text{SiO}_2$ (Fig. 3e and f) showed the presence of plate-like aggregates with porous structures and uneven surfaces. The morphology of the catalysts firmly rests on the used synthesis process. The ZnAl_2O_4 powders prepared with polyhedral morphology with the solid-state method by Du et al. [29] and zinc aluminate powders with rod-like-needles morphology synthesized by citrate sol-gel were investigated by Motloung et al. [30].

The SEM pictures of the samples showed that the particles of ZnAl_2O_4 based catalysts are nearly spherical with narrow particle size distribution. By comparing the images, it is evident that the size of the carbon nanotube nanoparticles is smaller than SiO_2 and thus its surface area is more significant, which increases the carbon nanotube photocatalytic performance. This is confirmed by the BET results that are presented in the next section. Both synthesized Zn-based catalysts displayed a solid affinity for agglomerate with plate-like morphology. As can be seen from Fig. 3 the average particle size of $\text{ZnAl}_2\text{O}_4/\text{SiO}_2$ and $\text{ZnAl}_2\text{O}_4/\text{CNT}$ samples was 22.18 and 35.1 nm, respectively.

3.5. Elemental analysis of the synthesized catalysts by EDX method

The EDX technique was used for chemical characterization and qualitative elemental analysis of samples [31,32]. The Zn-based catalysts were composed of Zn, Al, C, Si, and oxygen. The EDX spectra of $\text{ZnAl}_2\text{O}_4/\text{CNT}$ and $\text{ZnAl}_2\text{O}_4/\text{SiO}_2$ nanocomposites are presented in Figs. 4 and 5. It can be seen the presence of carbon, oxygen, aluminum and zinc elements in the $\text{ZnAl}_2\text{O}_4/\text{CNT}$ nanocomposite and the silicon, oxygen, aluminum and zinc elements in the $\text{ZnAl}_2\text{O}_4/\text{SiO}_2$ nanocomposites indicating the synthesis of these compounds and, more importantly, the absence of other compounds.

3.6. BET results of synthesized samples

The pore volume and specific surface area of the synthesized catalysts were determined by N_2 adsorption at -196°C .

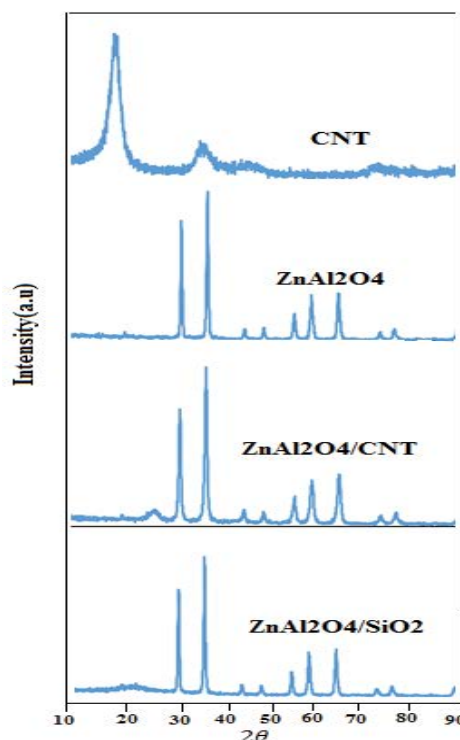


Fig. 2. XRD pattern of CNT, ZnAl_2O_4 , $\text{ZnAl}_2\text{O}_4/\text{CNT}$ and $\text{ZnAl}_2\text{O}_4/\text{SiO}_2$ sample.

BET analysis determines physical properties such as specific surface area, porosity and volume of cavities in many applications. Nitrogen adsorption–desorption isotherms for the two $\text{ZnAl}_2\text{O}_4/\text{SiO}_2$ and $\text{ZnAl}_2\text{O}_4/\text{CNT}$ samples show the highest surface area for $\text{ZnAl}_2\text{O}_4/\text{CNT}$ containing carbon nanotube compared to $\text{ZnAl}_2\text{O}_4/\text{SiO}_2$. The surface area, cavity size and cavity volume of the two samples are presented in Table 1. The specific surface area of the ZnAl_2O_4 catalyst was $80 \text{ m}^2 \text{ g}^{-1}$. The surface area of the ZnAl_2O_4 is significantly increased by adding carbon nanotube in the catalyst composition, which is essential due to the crucial role in the achievement of the reactive molecules in the catalytic materials. Furthermore, the BET surface area of the sample reduces with rising pore size, as presented in Table 1.

The results showed that the larger surface area provides more reaction or absorption sites during the photocatalytic reaction and improves the photocatalytic activity. The $\text{ZnAl}_2\text{O}_4/\text{CNT}$ powder presented a larger BET surface area ($201.81 \text{ m}^2 \text{ g}^{-1}$) and smaller pore size and pore volume than $\text{ZnAl}_2\text{O}_4/\text{SiO}_2$.

The catalytic performance of Pt- ZnAl_2O_4 on the n-butane dehydrogenation reaction was considered by Ballarini et al. [24], who determined that the ZnAl_2O_4 catalysts showed the best catalytic activity with higher BET surface area. In the present work, the porous structure and high surface area of $\text{ZnAl}_2\text{O}_4/\text{CNT}$ are of excessive significance for catalytic purposes.

3.7. Photoluminescence spectroscopy analysis

The PL analysis is a valuable tool for investigating the electrical, optical, and photoelectric properties of

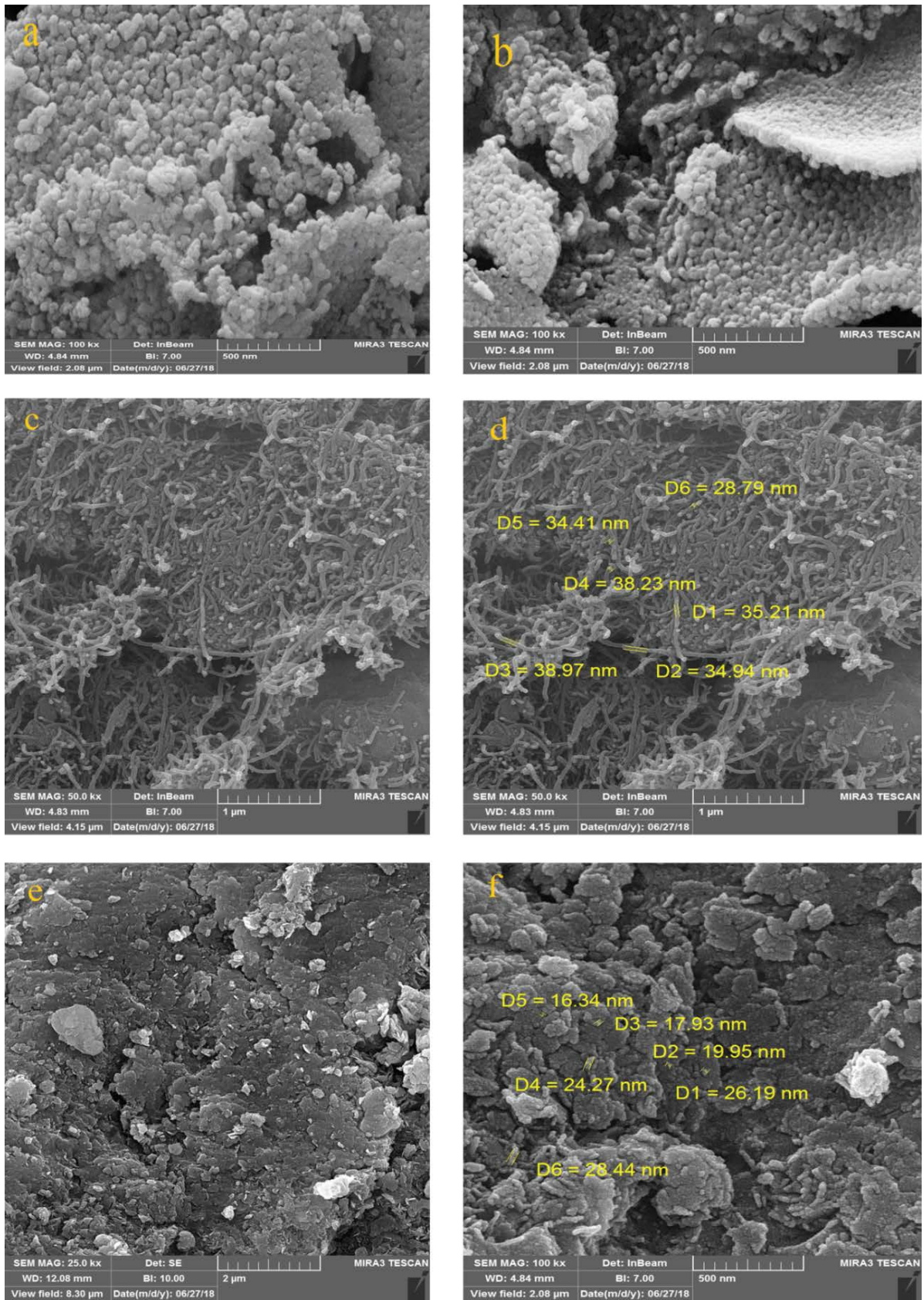
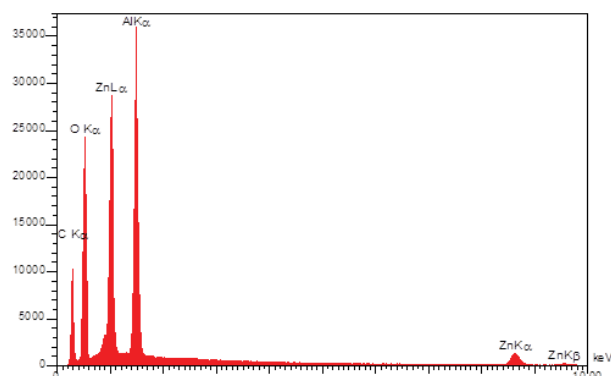
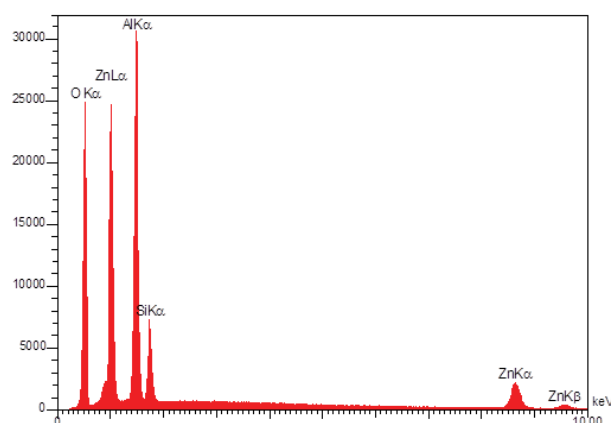
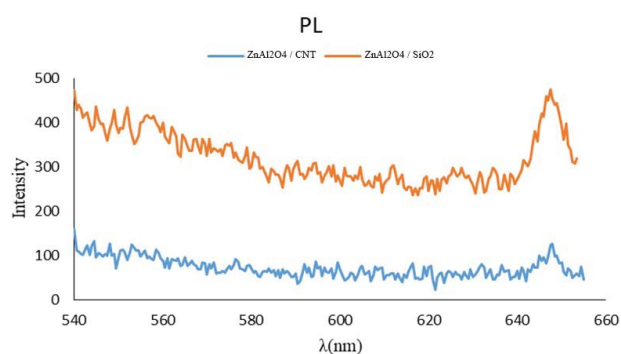


Fig. 3. SEM images of the synthesized photocatalysts: (a,b) ZnAl₂O₄ photocatalyst, (c,d) ZnAl₂O₄/CNT photocatalyst, and (e,f) ZnAl₂O₄/SiO₂ photocatalyst.

Fig. 4. EDX spectrum of ZnAl₂O₄/CNT photocatalyst.Fig. 5. EDX spectrum of ZnAl₂O₄/SiO₂ photocatalyst.Fig. 6. Photoluminescence spectrum (brown) of ZnAl₂O₄/SiO₂ and (blue) of ZnAl₂O₄/CNT.

semiconductor nanomaterial and a valuable method for understanding the processes occurring on the material surface. The improvement in the activity of photocatalysts and other nanocompound originated from a single up-conversion of graphene quantum dots or carbon has been investigated by many researchers [33,34]. Aleksandrak et al. [35] investigated the alteration of graphitic carbon nitride by graphene oxide and reduced graphene oxide

Table 1
Comparison of BET results in synthesized samples

Sample	ZnAl ₂ O ₄ /SiO ₂	ZnAl ₂ O ₄ /CNT
Surface area (m ² g ⁻¹)	94.59	201.81
Pore volume (cm ³ g ⁻¹)	0.773	0.427
Pore size (nm)	31.0	8.46

and their photocatalytic and photoluminescent was studied. Based on PL analysis, the recombination rate of the electron–hole pairs produced during the photocatalytic reaction can be studied. It can be noticed that the peak intensities recorded in this test were lower, so the recombination rate of the electron–cavity pairs will decrease and the separation efficiency will increase. This will lead to an increase in photocatalytic degradation of the pollutant. The PL spectrum of ZnAl₂O₄/SiO₂ and ZnAl₂O₄/CNT nanocomposites with excitation wavelength at 340 nm shows a sharp peak at 650 nm wavelength, which is higher in ZnAl₂O₄/SiO₂ nanocomposites than in ZnAl₂O₄/CNT, meaning that the ZnAl₂O₄/CNT sample has a lower electron–cavity recombination rate and higher separation efficiency. This would lead to increased photocatalytic degradation of the contaminant by the ZnAl₂O₄/CNT sample. It should be noted that the PL spectra of pure ZnAl₂O₄ are not shown in Fig. 6, but according to the results of other researchers [36], it was clear that it has a sharper peak than the peaks of ZnAl₂O₄/SiO₂ and ZnAl₂O₄/CNT sample at 650 nm, which showed that it has a higher electron–cavity recombination rate and consequently lower photocatalytic activity than the modified ones.

3.8. Effect of different photocatalysts on RhB

The UV-Vis absorption spectrum of Rhodamine B in aqueous solution in the presence of ZnAl₂O₄, ZnAl₂O₄/SiO₂ and ZnAl₂O₄/CNT nanocomposites showed that with an increase in irradiation time for all samples, the absorption intensity of dye at 554 nm was decreased. However, complete disappearance for ZnAl₂O₄/CNT occurred after 15 min of illumination (Fig. 7), but in the case, with ZnAl₂O₄ and ZnAl₂O₄/SiO₂ photocatalysts, the degradation efficiency after an hour was 40% and 47%, respectively. Since no new peak was observed in the UV-Vis spectrum, it can be concluded that in ZnAl₂O₄/CNT technique, all intermediate products formed have been destroyed.

The degradation efficiency is calculated by the following equation:

$$\text{Degradation efficiency} = \frac{(A_0 - A)}{A_0} \times 100 \quad (1)$$

where A_0 is the initial color concentration and A is the color concentration at time t . The color absorption capacity, bandgap energy, surface and structural properties of the catalyst, as well as the cavity–electron coupling energy produced in the photocatalytic process and their separation, are some of the critical parameters that influence the

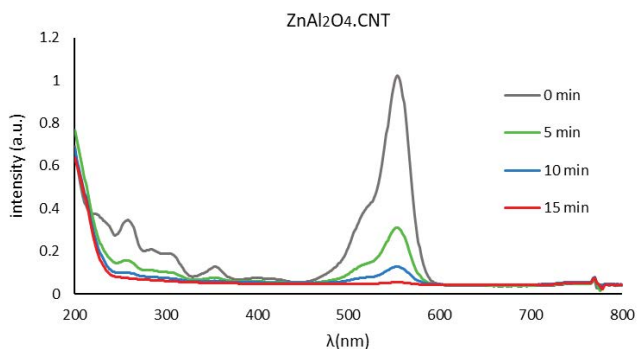


Fig. 7. UV-Vis spectrum of photocatalytic degradation of Rhodamine B (1×10^{-5} M) under UVA light and $\text{ZnAl}_2\text{O}_4/\text{CNT}$.

photocatalytic performance. The degradation of Rhodamine B on the CNT-nanocomposite sample is higher than that of other samples due to the intensive interactions between Rhodamine B and the carbon nanotube.

In the photocatalytic test, about 0.4 g of catalyst was mixed with a 500 mL RhB solution (1×10^{-5} M) at pH of 7, and an adsorptive test mainly continued in the dark for 30 min to reach desorption–absorption equilibrium of RhB on the catalyst surface before irradiation. After an interval of the arranged time, 3 mL of dye solution was withdrawn for concentration analysis, which was checked by UV-Vis spectrophotometer.

The degradation efficiencies of RhB for various samples under the UV-light were investigated and the results are presented in Fig. 8. Compared with the $\text{ZnAl}_2\text{O}_4/\text{SiO}_2$ particle, the improved photocatalytic property of $\text{ZnAl}_2\text{O}_4/\text{CNT}$ is related to the expansion of specific surface area to obtain more active sites which can play an important role in the absorption of UV-light. These findings are in agreement with the results of other researchers such as Xie et al., that they found out the photocatalytic activity of T/Z-5 is nearly 30% greater than that of T/Z-0 ones, showing that the combination of TiO_2 into ZrO_2 origins a slow recombination of electron-hole pair and rapid electron transfer [37].

3.9. Investigation of the intermediate reaction

Degradation of the organic pollutants by photocatalysts mostly can occur via the absorption of photo and generation of holes and electrons on the catalyst, the transmission of charge transporters, and the application of the charge transporters with reagents. $\text{ZnAl}_2\text{O}_4/\text{CNT}$ showed the capability to absorb UV light, and the electrons were transferred from the valance band (VB) to the conduction band (CB). The degradation of RhB was related to the photosensitized method, that is, the photon flux was absorbed on RhB at first and at that time, the electrons originated from the photo were shifted to the excited state of the RhB due to the $\pi-\pi^*$ intermolecular transition and subsequently caused the RhB to be oxidized. The electrons of the excited state were transferred rapidly to the CB of $\text{ZnAl}_2\text{O}_4/\text{CNT}$ [Eq. (2)] and then captured by molecular O_2 injected into the reactor [Eq. (7)]. The later reactions can result in the production of intermediates and subsequently

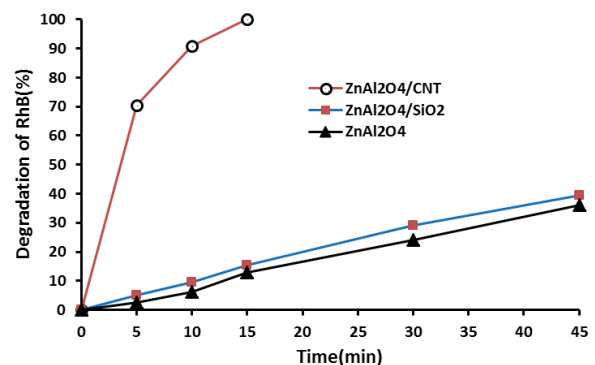
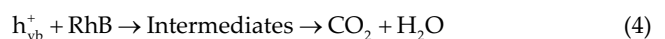


Fig. 8. The degradation efficiency of Rhodamine B using ZnAl_2O_4 (blue), $\text{ZnAl}_2\text{O}_4/\text{SiO}_2$ (Red) and $\text{ZnAl}_2\text{O}_4/\text{CNT}$ (green) along with UV-light.

mineralization of RhB. Perhaps the including reactions are as the succeeding [Eqs. (2)–(10)]:



The conduction band of photocatalyst has the same potential as oxygen regeneration potential. In many photocatalytic reactions, the adsorbed oxygen acts as a trap for the electrons in the conduction band and avoiding recombination of electrons and holes and subsequently decreasing active sites [Eq. (3)]. The transfer of electrons to oxygen is the speed limiting step in photocatalytic reaction [Eq. (7)], therefore the effect of oxygen concentration on this step was removed in all experiments using stirring, providing oxygen thru air pump or shallow selection of solutions inside reactors [38].

In heterogeneous photocatalytic processes, the cavities in the VB of the catalyst oxidize the water molecules of the hydroxide adsorbed on the catalyst's surface and produce hydroxyl radicals [Eq. (5)]. Oxidation of RhB molecules may occur both indirectly, through surface-bound hydroxyl radicals, and directly through the cavity of the VB before being trapped inside or at the surface of the catalyst. The electrons produced by the photocatalytic process at the CB may react with oxygen to form superoxide radicals ($\text{O}_2^{\bullet-}$) [Eq. (7)], and these radicals may form the peroxide of RhB or hydrogen peroxide [Eqs. (8)–(9)]. Intermediate compounds also react with hydroxyl radicals to form final mineral and nontoxic products such as water and carbon dioxide.





4. Conclusion

This study was performed to evaluate the photocatalytic degradation of Rhodamine B. Single-phase ZnAl_2O_4 spinel-type catalysts have been prepared by the direct method through hydrothermal technique without calcination. The $\text{ZnAl}_2\text{O}_4/\text{CNT}$ powder showed a larger BET surface area and smaller pore size and pore volume than $\text{ZnAl}_2\text{O}_4/\text{SiO}_2$. The results showed an improvement in the photocatalytic activity of composites compared to pure ZnAl_2O_4 . It was clear from FESEM that the size of $\text{ZnAl}_2\text{O}_4/\text{CNT}$ nanoparticles was smaller than that of $\text{ZnAl}_2\text{O}_4/\text{SiO}_2$ and consequently its surface area was greater.

The presence of reduced CNT improved the photocatalytic activity of ZnAl_2O_4 . The use of CNT as a catalyst substrate increased the surface area and subsequently catalyst performance. BET analysis showed that the larger surface area provides more adsorption sites during a photocatalytic reaction and thereby improves the photocatalytic activity.

The PL test showed that in the $\text{ZnAl}_2\text{O}_4/\text{CNT}$ sample, the recombination rate of the electron-hole pairs was lower and the separation efficiency was many times higher, which increased the photocatalytic efficiency.

The UV-Vis absorption spectrum of Rhodamine B in an aqueous solution showed that the dye was completely removed by $\text{ZnAl}_2\text{O}_4/\text{CNT}$ compared to the other photocatalysts, after 15 min of reaction. While in ZnAl_2O_4 and $\text{ZnAl}_2\text{O}_4/\text{SiO}_2$ runs, about 40% and 47% of the dye were removed after 1 h of reaction.

References

- [1] A. Shokri, Employing electrocoagulation for the removal of Acid Red 182 in aqueous environment by using Box-Behnken design method, *Desal. Water Treat.*, 115 (2018) 281–287.
- [2] A. Shokri, Removal of Acid red 33 from aqueous solution by Fenton and photo Fenton processes, *J. Chem. Health Risks*, 7 (2017) 119–131.
- [3] H.L. Jiang, P.H. Chen, S.L. Luo, X.B. Luo, X.M. Tu, Q. Cao, Y.L. Zhou, W.B. Zhang, Synthesis of novel biocompatible composite $\text{Fe}_3\text{O}_4/\text{ZrO}_2/\text{chitosan}$ and its application for dye removal, *J. Inorg. Organomet.*, 23 (2013) 393–400.
- [4] T.H. Wu, Q. Shao, S.S. Ge, L.W. Bao, Q.Y. Liu, The facile preparation of novel magnetic zirconia composites with the aid of carboxymethyl chitosan and their efficient removal of dye, *RSC Adv.*, 6 (2016) 58020–58027.
- [5] Z. Feng, L. Zeng, Q. Zhang, S. Ge, X. Zhao, H. Lin, Y. He, In situ preparation of $g\text{-C}_3\text{N}_4/\text{Bi}_2\text{O}_3/\text{I}_2$ complex and its elevated photoactivity in Methyl Orange degradation under visible light, *J. Environ. Sci.*, 87 (2020) 149–162.
- [6] Q. Zhang, P. Chen, L. Chen, M. Wu, X. Dai, P. Xing, H. Lin, L. Zhao, Y. He, Facile fabrication of novel $\text{Ag}_2\text{S}/\text{K-g-C}_3\text{N}_4$ composite and its enhanced performance in photocatalytic H_2 evolution, *J. Colloid Interface Sci.*, 568 (2020) 117–129.
- [7] Z. Fang, Q. Li, L. Su, J. Chen, K. Chou, X. Hou, Efficient synergy of photocatalysis and adsorption of hexavalent chromium and Rhodamine B over $\text{Al}_3\text{SiC}_4/\text{rGO}$ hybrid photocatalyst under visible-light irradiation, *Appl. Catal., B*, 241 (2019) 548–560.
- [8] M. Mohadesi, A. Shokri, Treatment of oil refinery wastewater by photo-Fenton process using Box–Behnken design method: kinetic study and energy consumption, *Int. J. Environ. Sci. Technol.*, 16 (2019) 7349–7356.
- [9] A. Shokri, Application of Sono-photo-Fenton process for degradation of phenol derivatives in petrochemical wastewater using full factorial design of experiment, *Int. J. Ind. Chem.*, 9 (2018b) 295–303.
- [10] A. Shokri, A kinetic study and application of electro Fenton process for the remediation of the aqueous environment containing Toluene in a batch reactor, *Russ. J. Appl. Chem.*, 90 (2017) 452–457.
- [11] M. Mohadesi, A. Shokri, Evaluation of Fenton and photo-Fenton processes for the removal of p-chloronitrobenzene in aqueous environment using Box–Behnken design method, *Desal. Water Treat.*, 81 (2017) 199–208.
- [12] S. Xing, S. Song, J. Xiang, Low temperature combustion synthesis and photoluminescence mechanism of $\text{ZnO}/\text{ZnAl}_2\text{O}_4$ composite phosphors, *Optik*, 208 (2020) 164526, doi: 10.1016/j.ijleo.2020.164526.
- [13] P. Chen, L. Chen, S. Ge, W. Zhang, M. Wu, P. Xing, T.B. Rotamond, H. Lin, Y. Wu, Y. He, Microwave heating preparation of phosphorus doped $g\text{-C}_3\text{N}_4$ and its enhanced performance for photocatalytic H_2 evolution in the help of Ag_3PO_4 nanoparticles, *Int. J. Hydrogen Energy*, 45 (2020) 14354–14367.
- [14] F.Z. Akika, M. Benamira, H.L. Ahmar, M. Trari, I.A. Vramova, Ş. Suzer, Structural and optical properties of Cu-doped ZnAl_2O_4 and its application as photocatalyst for Cr(VI) reduction under sunlight, *Surf. Interfaces*, 18 (2020) 100406, doi: 10.1016/j.surfint.2019.100406.
- [15] P. Moradipour, F. Dabirian, M. Moradipour, Ternary $\text{ZnO}/\text{ZnAl}_2\text{O}_4/\text{Al}_2\text{O}_3$ composite nanofiber as photocatalyst for conversion of CO_2 and CH_4 , *Ceram. Int.*, 46 (2020) 5566–5574.
- [16] A. Shokri, K. Mahanpoor, D. Soodbar, Evaluation of a modified TiO_2 (GO–B– TiO_2) photocatalyst for degradation of 4-nitrophenol in petrochemical wastewater by response surface methodology based on the central composite design, *J. Environ. Chem. Eng.*, 4 (2016) 585–598.
- [17] Z.F. Yin, C.J. Cui, H. Chen, Duoni, X. Yu, W.Z. Qian, The application of carbon nanotube/graphene-based nanomaterials in wastewater treatment, *Nano/Microscale Mater.*, 16 (2019) 1902301, doi: 10.1002/sml.201902301.
- [18] M. Taghioskoui, Trends in graphene research, *Mater. Today*, 12 (2009) 34–37.
- [19] A.R. Oganov, R.J. Hemley, R.M. Hazen, A.P. Jones, Structure, bonding, and mineralogy of carbon at extreme conditions, *Rev. Mineral. Geochem.*, 75 (2013) 47–77.
- [20] L. Mu, J. Wan, Z. Wang, Y. Gao, Y. Qian, Mn-doped zinc aluminate nanoparticles: hydrothermal synthesis, characterization, and photoluminescence properties, *J. Nanosci. Nanotechnol.*, 6 (2006) 863–867.
- [21] T. Charinpanitkul, P. Poommarin, A. Wongkaew, K.S. Kim, Dependence of zinc aluminate microscopic structure on its synthesis, *J. Ind. Eng. Chem.*, 15 (2009) 163–166.
- [22] S. Farhadi, S. Panahandehjoo, Spinel-type zinc aluminate (ZnAl_2O_4) nanoparticles prepared by the co-precipitation method: a novel, green and recyclable heterogeneous catalyst for the acetylation of amines, alcohols and phenols under solvent-free conditions, *Appl. Catal., A*, 382 (2010) 293–302.
- [23] A. Adan-Mas, D. Wei, Photoelectrochemical properties of graphene and its derivatives, *Nanomaterials*, 3 (2013) 325–356.
- [24] A.D. Ballarini, S.A. Bocanegra, A.A. Castro, S.R. De Miguel, O.A. Scelza, Characterization of ZnAl_2O_4 obtained by different methods and used as catalytic support of Pt, *Catal. Lett.*, 129 (2009) 293–302.
- [25] Y. Wang, J. Liu, L. Liu, D.D. Sun, Enhancing stability and photocatalytic activity of ZnO nanoparticles by surface modification of graphene oxide, *J. Nanosci. Nanotechnol.*, 12 (2012) 3896–3902.

- [26] S.F. Wang, G.Z. Sun, L.M. Fang, L. Lei, X. Xiang, X.T. Zu, A comparative study of $ZnAl_2O_4$ nanoparticles synthesized from different aluminium salts for use as fluorescence materials, *Sci. Rep.*, 5 (2015) 12849, doi: 10.1038/srep12849.
- [27] K.R. Reddy, K.V. Karthik, S.B. Benaka Prasad, S.K. Soni, H.M. Jeong, Enhanced photocatalytic activity of nanostructured titanium dioxide/polyaniline hybrid photocatalysts, *Polyhedron*, 120 (2016) 169–174.
- [28] M.R. Quirino, M.J.C. Oliveira, D. Keyson, G.L. Lucena, J.B.L. Oliveira, L. Gama, Synthesis of zinc aluminate with high surface area by microwave hydrothermal method applied in the transesterification of soybean oil (biodiesel), *Mater. Res. Bull.*, 74 (2016) 124–128.
- [29] X. Du, L. Li, W. Zhang, W. Chen, Y. Cui, Morphology and structure features of $ZnAl_2O_4$ spinel nanoparticles prepared by matrixisolation-assisted calcination, *Mater. Res. Bull.*, 61 (2015) 64–69.
- [30] S.V. Motloung, F.B. Dejene, H.C. Swart, O.M. Ntwaeaborwa, Effects of Zn/citric acid mole fraction on the structure and luminescence properties of the un-doped and 1.5% Pb^{2+} doped $ZnAl_2O_4$ powders synthesized by citrate sol–gel method, *J. Lumin.*, 163 (2015) 8–16.
- [31] K. Wang, L. Jiang, X. Wu, G. Zhang, Vacancy mediated Z-scheme charge transfer in a 2D/2D $La_2Ti_2O_7/g-C_3N_4$ nanojunction as a bifunctional photocatalyst for solar-to-energy conversion, *J. Mater. Chem. A*, 8 (2020) 13241–13247.
- [32] Y. Wang, K. Wang, J. Wang, X.W.G. Zhang, $Sb_2WO_6/BiOBr$ 2D nanocomposite S-scheme photocatalyst for $\dot{N}O$ removal, *J. Mater. Sci. Technol.*, 56 (2020) 236–243.
- [33] Y. Hao, X. Dong, X. Wang, S. Zhai, H. Ma, X. Zhang, Controllable electrostatic self-assembly of sub-3 nm graphene quantum dots incorporated into mesoporous Bi_2MoO_6 frameworks: efficient physical and chemical simultaneous co-catalysis for photocatalytic oxidation, *J. Mater. Chem. A*, 4 (2016) 8298–8307.
- [34] H. Zhang, L. Zhao, F. Geng, L.H. Guo, B. Wan, Y. Yang, Carbon dots decorated graphitic carbon nitride as an efficient metal-free photocatalyst for phenol degradation, *Appl. Catal. B*, 180 (2016) 656–662.
- [35] M. Aleksandrak, W. Kukulka, E. Mijowska, Graphitic carbon nitride/graphene oxide/reduced graphene oxide nanocomposites for photoluminescence and photocatalysis, *Appl. Surf. Sci.*, 398 (2017) 56–62.
- [36] D. Zhang, C. Wang, Y. Liu, Q. Shi, W. Wang, Y. Zhai, Green and red photoluminescence from $ZnAl_2O_4:Mn$ phosphors prepared by sol–gel method, *J. Lumin.*, 132 (2012) 1529–1531.
- [37] W. Xie, R. Li, Q.Y. Xu, Enhanced photocatalytic activity of Se-doped TiO_2 under visible light irradiation, *Sci. Rep.*, 8 (2018) 8752, doi: 10.1038/s41598-018-27135-4.
- [38] T.T.T. Dang, S.T.T. Le, D. Channei, W. Khanitchaidecha, Photodegradation mechanisms of phenol in the photocatalytic process, *Res. Chem. Intermed.*, 42 (2016) 5961–5974.